Effects of Objective Numerical Apertures on Achievable Imaging Depths in Multiphoton Microscopy

CHIH-KUAN TUNG,[1] YEN SUN,[1] WEN LO,[1] SUNG-JAN LIN,[2,3] SHIOU-HWA JEE,[3,4] AND CHEN-YUAN DONG[1]*

[1]*Department of Physics, National Taiwan University, Taipei 106, Taiwan*
[2]*Institute of Biomedical Engineering, College of Medicine and College of Engineering, National Taiwan University, Taipei 100, Taiwan*
[3]*Department of Dermatology, National Taiwan University Hospital, Taipei 100, Taiwan*
[4]*Department of Dermatology, National Taiwan University College of Medicine, Taipei 100, Taiwan*

KEY WORDS multiphoton microscopy; numerical aperture; spherical aberration; scattering

ABSTRACT Multiphoton microscopy is a powerful technique for achieving three-dimensional submicron imaging in biological specimens. However, specimen optical parameters such as refractive indices and scattering coefficients can result in the loss of image resolution and decreased signal in depth. These factors are coupled to the focusing objective's numerical aperture (NA) in limiting the achievable imaging depths. In this work, we performed multiphoton imaging on aqueous fluorescent solution, human skin, and rat tail tendon to show that, under the same immersion condition, lower NA objectives can examine more deeply into biological specimens and should be used when optimal imaging depths is desired. *Microsc. Res. Tech. 65:308–314, 2004.*

INTRODUCTION

The introduction of multiphoton microscopy in the early 1990s revolutionized biological optical microscopy (Denk et al., 1990). Increased image contrast, reduced photodamage, and enhanced depth penetration are some of the major advantages of nonlinear optical microscopy (Centonze and White, 1998; So et al., 2000). Many areas of biology and medicine benefited from this development and multiphoton microscopy has found wide applications in areas such as tissue imaging, neurobiology, developmental biology, oncology, and drug delivery (Brown et al., 2001; Masters et al., 1997; Piston et al., 1995; Squirrel et al., 1999; Sun et al., 2003; Svoboda et al., 1997; Yu et al., 2001; Yuste and Denk, 1995). In many of these studies, the key advantage of multiphoton microscopy is its ability to image deep into the biological specimens (ex vivo or in vivo) without disruptive histological procedures. As a result, temporal evolution of physiological phenomena can be continuously traced. In most applications using multiphoton techniques, two sample excitation modes are involved. The first mechanism involves the simultaneous absorption of two or more near-infrared excitation photons. Since the selection rules for such a process can be different from the one-photon excitation process, multiphoton fluorescence excitation processes tend to excite states with odd parity (odd number of photons absorbed) or even parity (even number of photons absorbed) from the ground state specimens. In such in-depth optical imaging of biological specimens, the effects of refractive index induced spherical aberration and scattering can contribute more significantly to a degradation of image resolution and reduced signal strength from deep within tissues.

While it is difficult to separate the effects of spherical aberration and scattering in multiphoton imaging of biological specimens, various attempts have been made to characterize the effects of refractive index mismatch and scattering in multiphoton imaging. Imaging of tissue-like constructs demonstrated that spherical aberration from index mismatch results in resolution degradation and the effects worsen with increasing imaging depths. Tissue-like scattering, on the other hand, has been shown to decrease the amount of detectable fluorescence in depth. However, up to the typical imaging depths achievable in multiphoton microscopy, scattering does not appear to degrade the imaging point-spread-function (de Grauw et al., 1999; Dong et al., 2003; Dunn et al., 2003; Gerritsen and de Grauw, 1999). While it has been demonstrated that the proper choice of immersion objective can affect the achievable imaging depths in biological specimens, to the best of our knowledge the effects of the objective's numerical aperture (NA) on the achievable imaging depths using multiphoton microscopy have not been examined (Dong et al., 2004).

In multiphoton microscopy, the objective's NA can contribute to two optical electronic states. The excited molecules then undergo fluorescence emission which can be used for biomedical imaging applications. The second mechanism involves the polarization effects known as harmonic generation. If the polarization of the specimen of interest responds nonlinearly to the incident electric field, the polarization P_i can be expressed as:

$$P_i = \chi_{ij} E_j + \chi_{ijk} E_j E_k + \chi_{ijkl} E_j E_k E_l + \ldots \qquad [1]$$

C.-K. Tung and Y. Sun contributed equally to this work.

*Correspondence to: C.-Y. Dong, Department of Physics, National Taiwan University, Taipei 106, Taiwan.

Received 1 May 2004; accepted in revised form 9 September 2004
DOI 10.1002/jemt.20116
Published online in Wiley InterScience (www.interscience.wiley.com).

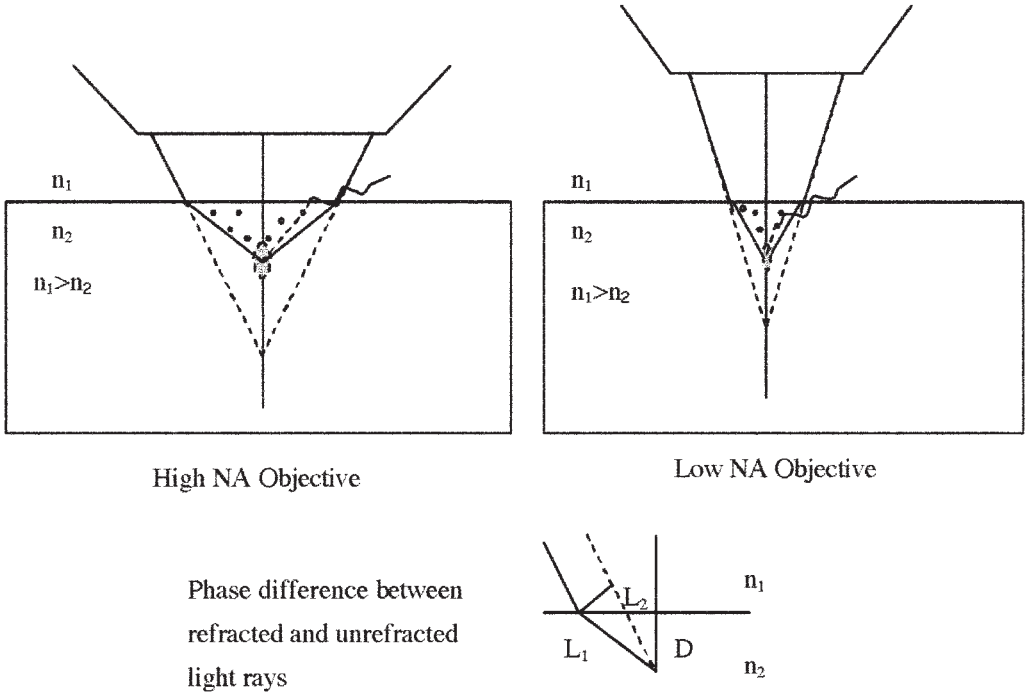

Fig. 1. The effects of numerical aperture on optical microscopy. In focusing to the same imaging depth, the light rays travel through less of the specimen for lower NA objectives. Refractive index mismatch induced spherical aberration and scattering are more significant for high NA objectives.

where χ_{ij}, χ_{ijk}, and χ_{ijkl} are the first-, second-, and third-order susceptibility tensors, respectively. In the case of nonvanishing second- and third-order susceptibility tensors, the specimen can respond to the incident excitation photons by producing photons at, respectively, one-half and one-third of the incident wavelength. In the case of second-harmonic generation, the physics dictate that the molecular structures producing the SHG photons need to be non-centrosymmetric in nature. Biological structures such as collagen and muscle fibers have been demonstrated to be strong generators of SHG signals (Campagnola and Loew, 2003; Stoller et al., 2002; Yeh et al., 2002; Zipfel et al., 2003; Zoumi et al., 2002).

Regardless of the excitation mechanisms, the effects of a specimen's optical properties on image quality are more pronounced in multiphoton microscopy. Unlike conventional microscopy, in which thick tissue sections or cell monolayers are the targets of study, multiphoton microscopy often image hundreds of microns into the phenomena capable of resolution degradation and signal reduction. First, since there exist longer optical paths for photons involved in the excitation and signal collection processes in higher NA objectives, one would expect scattering to result in an additional loss of fluorescence signal when high NA objectives are used to measure fluorescence signals from the same depth. On the other hand, one would also expect the differences in path lengths between objectives of different NAs to have an effect on refractive index mismatch induced spherical aberration. It has been shown that in the presence of spherical aberration the point-spread-function (PSF) needs to be modified to include a pupil function accounting for the different path lengths traveled by differently angled light rays (of wavelength λ) emerging from the index mismatching interface. Such modified PSF is given by:

$$I(u,v,D) = \left| \int_0^1 P(\rho,D) e^{iup^2/2} J_0(v\rho)\rho d\rho \right|^2 \qquad [2]$$

where $P(\rho,D) = e^{ik\Phi(\rho,D)}$ and $\Phi(\rho,D) = 2\pi D/\lambda\ n_1 \sin\alpha_1[\sqrt{csc^2\ \alpha_2 - \rho^2} - \sqrt{csc^2\ \alpha_1 - \rho^2}]$ depict the pupil function under such aberration. In this formalism, L_1, L_2, and D are the aberrated path length, unaberrated path length, and the distance from the interface to the focal plane, respectively. Furthermore, $u = 2\pi/\lambda\ (NA)^2 z$ and $v = 2\pi/\lambda\ (NA) r$ are the respective normalized axial and radial coordinates with z and r as the axial and radial spatial coordinates, respectively. In addition, $n_1 \sin\alpha_1 = n_2 \sin\alpha_2$ determines the relationship between α_1 (largest subtended angle of the objective) and α_2. The physical geometry of focusing through an index mismatched interface is illustrated in Figure 1 (Booth et al., 1998; Booth and Wilson, 2000). Intuitively, the longer path lengths of higher NA objectives will lead to the interference of light waves with additional phases and one would expect that a degradation of PSF will result. However, a characterization of the effects of NA on spherical aberration requires computation of Eq. 2 for the multiphoton case. In the two-photon case, $I^2(u,v,D)$ needs to be calculated. In biological specimens with varying refractive indices, the required computation can be complicated. For example,

in the case of skin the refractive indices change from about 1.47 in the stratum corneum to 1.43 in the granular layer. The indices of refraction further decreases to around 1.34 in the basal layer and again increases to about 1.41 in the dermis. In comparison, the scattering coefficient is 1–1.5 mm^{-1} in the stratum corneum and increases rapidly to 6–7 mm^{-1} in the granular layer. It further changes to 4–5 mm^{-1} near the basal region and approaches 5–8 mm^{-1} in the dermis (Knüttel and Boehlau-Godau, 2000; Tearney et al., 1995). On the other hand, a different biological specimen such as the rat tail tendon has a different index of refraction of around 1.5, a much less complicated refractive index structure in comparison (Stoller et al., 2003).

Nonetheless, the question of how the objective numerical apertures affect multiphoton imaging in-depth can be addressed by comparing the images and the multiphoton generated signal detected at different imaging depths by using the different objectives. In this work, we examine the effects of NA on achievable multiphoton imaging depths by comparing the axial integrated fluorescence strength acquired by different NA objectives using the same immersion fluids. Specifically, we used oil immersion objectives with NAs of 0.75 and 1.4 and water immersion objectives with NAs of 0.75 and 1.2. Our results will help researchers in choosing the proper objective to be used in multiphoton imaging experiments at increased depths.

MATERIALS AND METHODS

The multiphoton microscope used for this study is similar to a system described previously (Sun et al., 2003). In short, it is a home-built system based on a modified upright microscope (E800, Nikon, Japan). A diode-pumped (Millennia X, Spectra Physics, Mountain View, CA) titanium sapphire laser (Tsunami, Spectra Physics) was used as the excitation source. A galvonometer driven x-y scanner (Model 6220, Cambridge Technology, Cambridge, MA) is used to scan the excitation beam across the sample in a two-dimensional fashion. In combination with a motor-driven objective positioner for controlling the focal spot at different imaging depths (Prior Scientific, UK), a 3D image of the specimen can be obtained. In our study, we imaged three specimens using different objectives. The first sample was a uniform sulforhodamine B solution (in PBS buffer) 0.01 mM in concentration. The second specimen was a sulforhodamine B-treated skin. The skin used was immersed in a labeling solution consisting of 47.5% PBS buffer, 47.5% ethanol, 5% oleic acid, and sulforhodamine B was added at a concentration of 0.5 mg/ml. The skin was immersed in the labeling solution for 24 hours prior to being removed and mounted for multiphoton imaging. The final specimen we examined was rat tail tendon. This sample is made primarily of collagen fibers and we induced second-harmonic generation signal from the collagen. For all specimens, No. 1.5 thickness cover glasses were used to mount the specimens for viewing. A wavelength of 780 nm was used for all three samples. A dichroic mirror (720DCSPXR, Chroma Technology, Brattleboro, VT) was used to reflect the excitation source into the focusing objective. This short-pass dichroic mirror allows broadband fluorescence and second-harmonic generation signal to be transmitted. An additional filter (E680, Chroma Technology) was used to further attenuate the excitation wavelengths. For the sulforhodamine B solution and the sulforhodamine B-treated skin, an additional bandpass filter (HQ590/80, Chroma Technology) was used for fluorescence detection. In the case of rat tail tendon, a bandpass filter (HQ390/20, Chroma Technology) was used to isolate the second-harmonic generation signal. Single-photon counting PMT's (R7400P, Hamamatsu, Japan) were used for detection in our system.

The objectives chosen for this study are: 1) 20× Plan Fluor multi-immersion NA 0.75 (Nikon), 60× Plan Apo oil immersion NA 1.4 (Nikon), and 60× water Plan Apo NA 1.2 (Nikon). In the case of the multi-immersion 20× objective, water and oil immersion conditions were used. The power used for different specimens are different for different objectives. However, the maximum power was slightly over 10 mW for each sample. We tested the fluorescence or SHG signal for signal saturation and we chose the excitation power level that did not result in signal saturation. For the skin and tendon specimens, we also verified that the power levels used did not result in photobleaching. Linearly polarized light was used to excite the sulforhodamine B/PBS and the skin specimens while circularly polarized light was used to excite the rat tail tendon sample. The reason for using circularly polarized excitation is to ensure uniform excitation of the collagen fibers oriented at different orientations. Since the rat tail tendon tend to be homogeneous structurally, we dried 10-μm orange fluorescent microspheres (F8833, Molecular Probes, Eugene, OR) onto the cover glass prior to mounting the cover glass onto tendon. The microspheres were then used for position verification in imaging the same region of the specimen.

RESULTS AND DISCUSSION

The first data we present are the normalized axial fluorescence profiles of sulforhodamine B/PBS solution shown in Figure 2. The profiles obtained using 20× oil, 60× water, and 60× oil lenses are normalized to that obtained using the 20× water objective. The results plotted in Figure 2 show that the fluorescence profiles obtained using the 20× water and 60× water objectives overlap well with each other and show no signs of decay up to the imaging depth of 90 μm. This is not surprising, since both objectives were of the water immersion type and no PSF degradation is expected when imaging into a uniformly fluorescent, aqueous solution using water objectives. However, what is surprising is that the profile obtained using the 20× oil lens also overlaps well with that of the water objective results. This result supports the conclusion that index matching in multiphoton imaging may not be significant if the objective NA is not large. Our result is further supported by the fluorescence profile obtained using the 60× oil lens. In this case, the axial fluorescence profile clearly shows decay in the signal strength with increasing imaging depths. To be specific, compared to the surface fluorescence signal, the signal strength obtained at 60 μm is ~0.6 of that at the specimen surface. Since the sample does not contain scattering particles, the effects demonstrated are only due to the spherical aberration from refractive index mismatch. And our results seem to indicate that if achievable imaging depths rather than

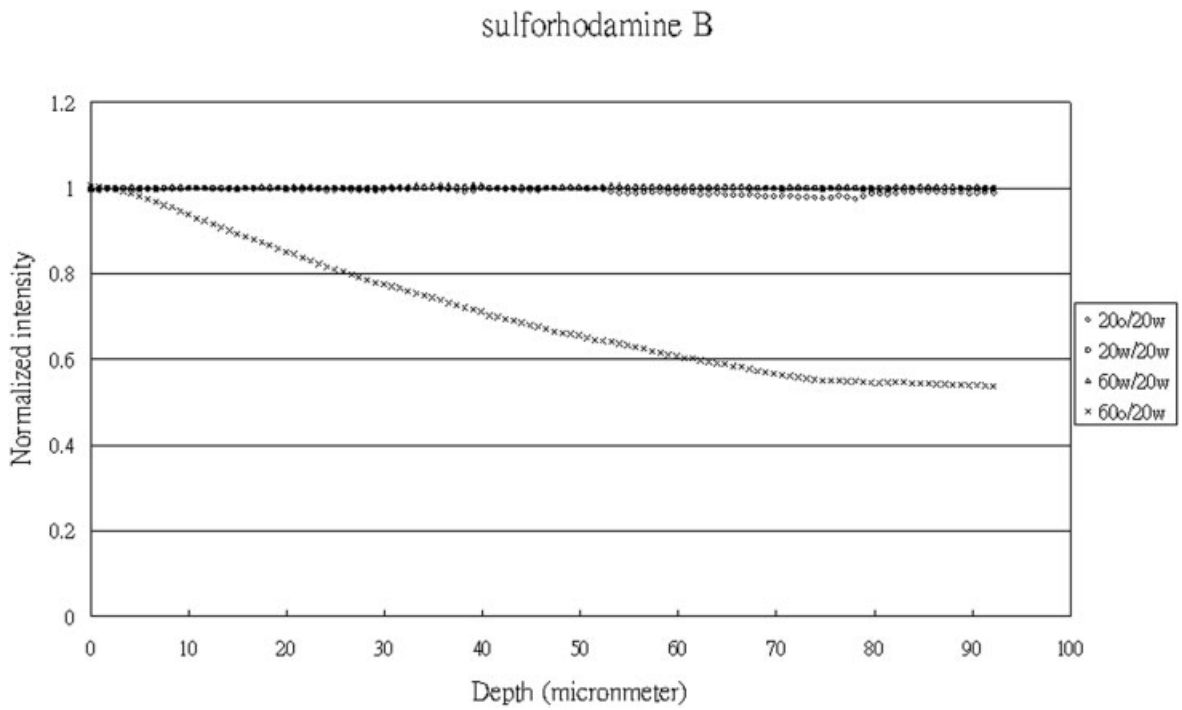

Fig. 2. Axial fluorescence profile of sulforhodamine B dissolved in PBS buffer. The fluorescence intensity measured with 20× water, 20× oil, 60× water, and 60× oil immersion objectives are normalized to that of the 20× water objective result.

image resolution is the primary goal in a particular multiphoton application, lower NA objectives should be used.

This observation can also be tested in biological specimens. The images and axial fluorescence profiles of sulforhodamine B-labeled skin are acquired using the same objectives described above and the results are shown in Figure 3. As discussed above, the optical properties of the skin are complicated. Nonetheless, both the images and the axial fluorescence profiles support the same conclusion as in the case for uniform aqueous sulrohdamine B solution. In this case, the images and fluorescence profiles (normalized to that obtained with the 20× oil objective) show that the profiles obtained using the 20× oil objective showed the least signal decay with increasing imaging depths followed by the 20× water lens. The results for the higher NA objectives are more complicated. At imaging depths less than about 12 μm, the 60× oil objective showed a slower degradation of image brightness with increasing depths. However, between about 12 and 23 μm the fluorescence measured using the 60× water objective is slightly higher than that obtained with the 60× oil lens. The trend is reversed as we imaged from 23 to 32 μm, where the 60× oil lens performed better than the 60× water objective. Finally, from 32 to 45 μm, the 60× water lens measured stronger fluorescence.

Shown in Figure 4 are the second-harmonic generation images and normalized signal (relative to that of the 20× oil data) obtained from the rat tail tendon at different imaging depths. In this case, similar to the results for the skin data, the images and the profiles obtained using the 20× oil objective decayed the slowest with increasing depths followed by the 20× water lens data. Although the results for the high NA objectives showed variations with different imaging depths, the 60× oil immersion objective consistently measured stronger SHG signal up to an imaging depth of 50 μm.

The variations in effective fluorescence measured for the high NA water and oil objectives are complicated by two factors. First, optical parameters such as refractive indices and scattering coefficients may not be uniform for biological specimens. Furthermore, the NAs for the high NA water and oil lenses are different. They are 1.2 and 1.4 for the 60× water and oil objectives, respectively. Therefore, in addition to satisfying index-matching conditions, one would expect that sample spherical aberration and scattering are more serious for the oil than the water objective. Nonetheless, the observation that under the same immersion conditions, lower NA objectives can image deeper into biological specimens than higher NA lenses remains valid for all the samples examined in this study.

CONCLUSIONS

In this work, we compared the images and/or axial signal profiles generated using multiphoton microscopy. In the three samples examined (aqueous solution, human skin, and rat tail tendon), lower NA objectives (0.75) can image deeper into the specimens than higher NA lenses (water: 1.2; oil: 1.4). Our results show that if obtainable imaging depths rather than image resolution is of primary consideration in multiphoton imag-

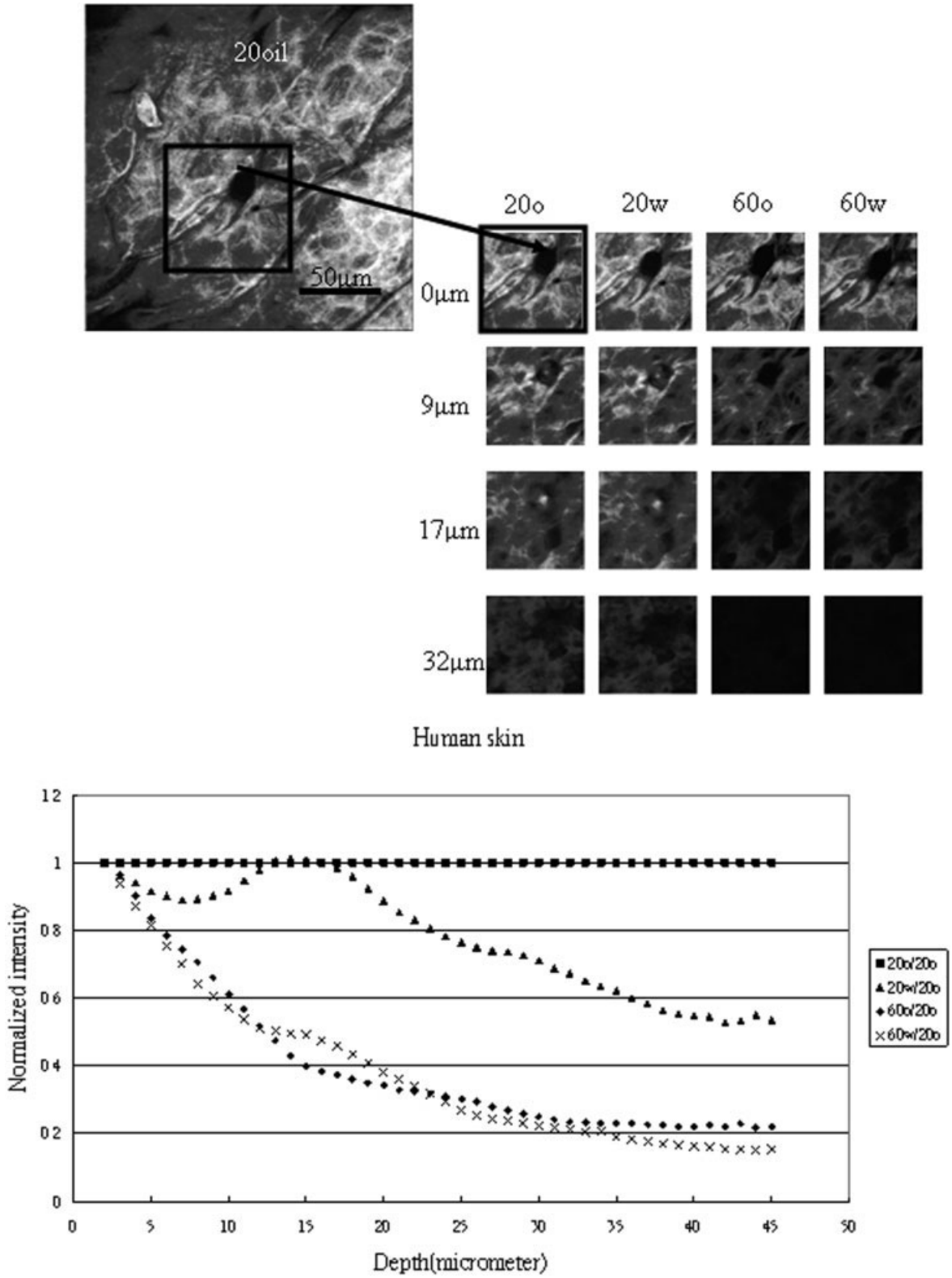

Fig. 3. Multiphoton imaging of fluorescently labeled skin acquired using the 20× water, 20× oil, 60× water, and 60× oil immersion objectives. The images and axial fluorescence intensity profiles for the same area of the skin are compared.

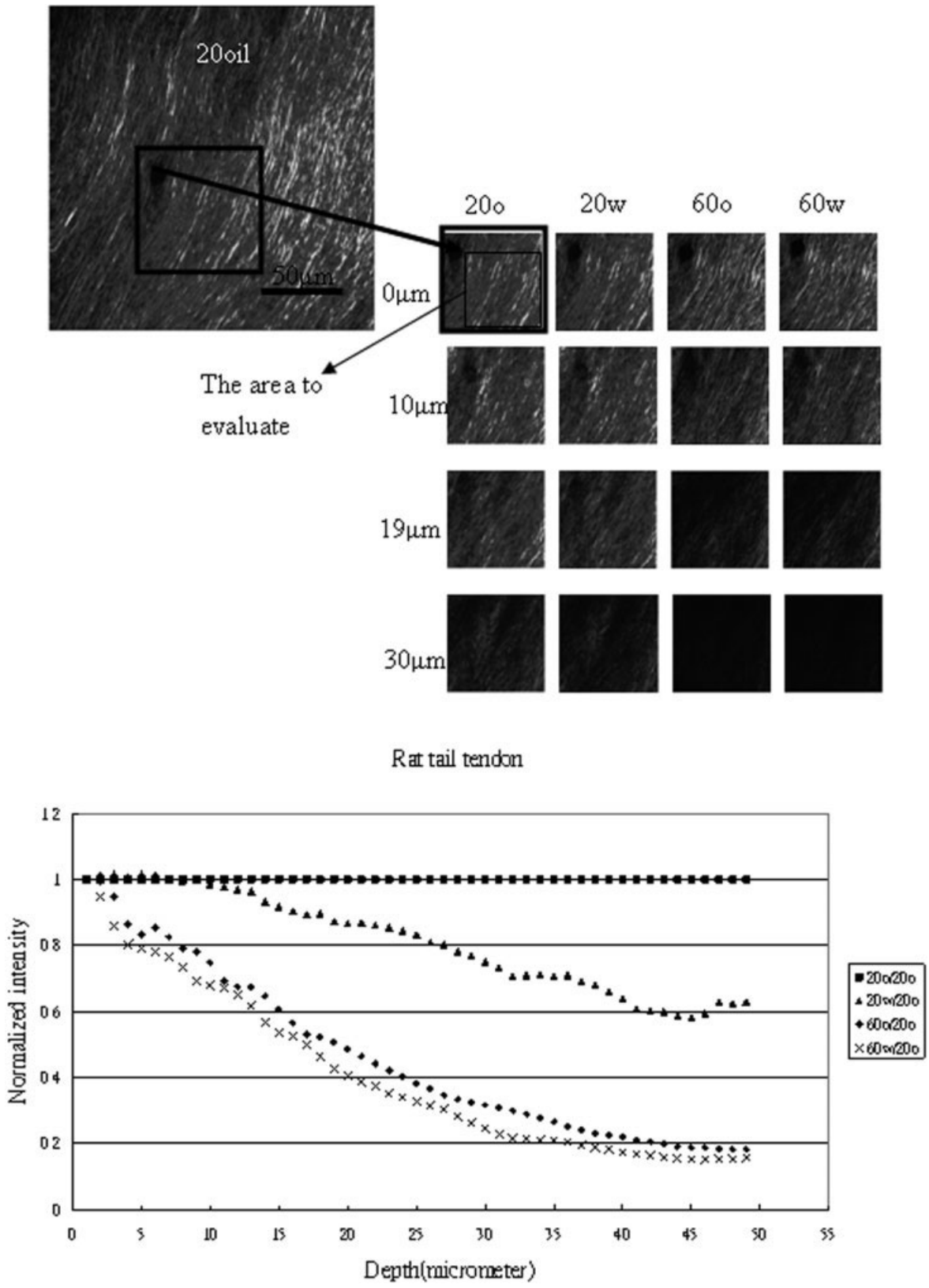

Fig. 4. Second-harmonic generation (SHG) images of rat tail tendon (at 390 nm) acquired using the 20× water, 20× oil, 60× water, and 60× oil immersion objectives. The images and axial SHG intensity profiles for the same area of the rat tail tendon are imaged and compared.

ing applications, lower NA objectives should be chosen over higher NA lenses.

REFERENCES

Booth MJ, Wilson T. 2000. Strategies for the compensation of specimen-induced spherical aberration in confocal microscopy of skin. J Microsc Oxford 200:68–74.

Booth MJ, Neil MAA, Wilson T. 1998. Aberration correction for confocal imaging in refractive-index-mismatched media. J Microsc Oxford 192:90–98.

Brown ED, Campbell RB, Tsuzuki Y, Xu L, Carmeliet P, Fukumura D, Jain RK. 2001. In vivo measurement of gene expression, angiogenesis and physiological function in tumors using multiphoton laser scanning microscopy. Nat Med 7:864–868.

Campagnola PJ, Loew LM. 2003. Second-harmonic imaging microscopy for visualizing biomolecular arrays in cells, tissues and organisms. Nat Biotechnol 21:1356–1360.

Centonze VE, White JG. 1998. Multiphoton excitation provides optical sections from deeper with scattering specimens than confocal imaging. Biophys J 75:2015–2024.

de Grauw CJ, Vroom JM, van der Voort HTM, Gerritsen HC. 1999. Imaging properties of two-photon excitation microscopy and effects of refractive-index mismatch in thick specimens. Appl Optics 38: 5995–6003.

Denk W, Strickler JH, Webb WW. 1990. Two-photon laser scanning fluorescence microscopy. Science 248:73–76.

Dong CY, Koenig K, So PTC. 2003. Characterizing point spread functions of two-photon fluorescence microscopy in turbid medium. J Biomed Optics 8:450–459.

Dong CY, Yu B, Kaplan PD, So PTC. 2004. Performances of high numerical aperature water and oil immersion objectives in deep-tissue, Multiphoton microscopic imaging of excised human skin, Microsc Res Tech. 63:81–86.

Dunn AK, Wallace VP, Coleno M, Berns MW, Tromberg BJ. 2000. Influence of optical properties on two-photon fluorescence imaging in turbid samples. Appl Optics 39:1194–1201.

Gerritsen HC, de Grauw CJ. 1999. Imaging of optically thick specimen using two-photon excitation microscopy. Microsc Res Tech 47:206–209.

Knüttel A, Boehlau-Godau M. 2000. Spatially confined and temporally resolved refractive index and scattering evaluation in human skin performed with optical coherence tomography. J Biomed Optics 5:83–92.

Masters BR, So PTC, Gratton E. 1997. Multiphoton excitation fluorescence microscopy and spectroscopy of in vivo human skin. Biophys J 72:2405–2412.

Piston DW, Masters BR, Webb WW. 1995. Three-dimensionally resolved NAD(P)H cellular metabolic redox imaging of the in situ cornea with two-photon excitation laser scanning microscopy. J Microsc 178:20–27.

So PTC, Dong CY, Masters BR, Berland KM. 2000. Two-photon excitation fluorescence microscopy. In: Annual review of biomedical engineering, vol. 2. Palo Alto; Annual Reviews. p 399–429.

Squirrell JM, Wokosin DL, White JG, Bavister BD. 1999. Long-term two-photon fluorescence imaging of mammalian embryos without compromising viability. Nat Biotechnol 17:763–767.

Stoller P, Reiser KM, Celliers PM, Rubenchik AM. 2002. Polarization-modulated second harmonic generation in collagen. Biophys J 82: 3330–3342.

Stoller P, Celliers PM, Reiser KM, Rubenchik AM. 2003. Quantitative second-harmonic generation microscopy in collagen. Appl Optics 42:5209–5219.

Sun Y, Su JW, Lo W, Lin SJ, Jee SH, Dong CY. 2003. Multiphoton polarization imaging of the stratum corneum and the dermais in ex-vivo human skin. Optics Express 11:3377–3384.

Svoboda K, Denk W, Kleinfeld D, Tank DW. 1997. In vivo dendritic calcium dynamics in neocortical pyramidal neurons. Nature 385: 161–165.

Tearney GJ, Brezinski ME, Southern JF, Bouma BE, Hee MR, Fujimoto JG. 1995. Determination of the refractive index of highly scattering human tissue by optical coherence tomography. Optics Lett 20:2258–2260.

Yu B, Dong CY, So PTC, Blankschtein D, Langer R. 2001. In vitro visualization and quantification of oleic acid induced changes in transdermal transport using two-photon fluorescence microscopy. J Invest Dermatol 117:16–25.

Yuste R, Denk W. 1995. Dendritic spines as basic functional units of neuronal integration. Nature 375:682–684.

Yeh AT, Nassif N, Zoumi A, Tromberg BJ. 2002. Selective corneal imaging using combined second-harmonic generation and two-photon excited fluorescence. Optics Lett 27:2082–2084.

Zipfel WR, Williams RM, Christie R, Nikitin AY, Hyman BT, Webb WW. 2003. Live tissue intrinsic emission microscopy using multiphoton-excited native fluorescence and second harmonic generation. Proc Natl Acad Sci USA 100:7075–7080.

Zoumi A, Yeh A, Tromberg BJ. 2002. Imaging cells and extracellular matrix in vivo by using second-harmonic generation and two-photon excited fluorescence. Proc Natl Acad Sci USA 99:11014–11019.